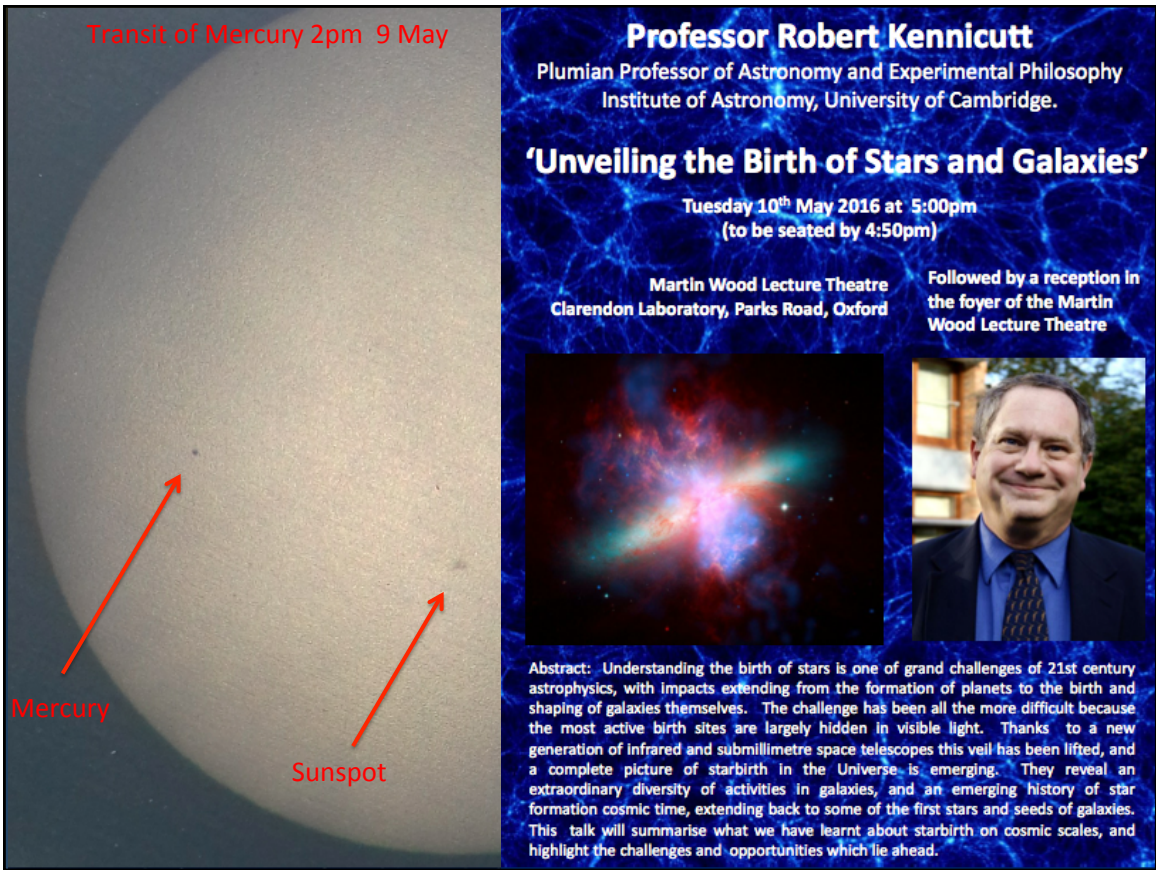

Professor Robert Kennicutt

Plumian Professor of Astronomy and Experimental Philosophy
Institute of Astronomy, University of Cambridge.

'Unveiling the Birth of Stars and Galaxies'

Tuesday 10th May 2016 at 5:00pm
(to be seated by 4:50pm)

Martin Wood Lecture Theatre
Clarendon Laboratory, Parks Road, Oxford

Followed by a reception in the foyer of the Martin Wood Lecture Theatre

Abstract: Understanding the birth of stars is one of grand challenges of 21st century astrophysics, with impacts extending from the formation of planets to the birth and shaping of galaxies themselves. The challenge has been all the more difficult because the most active birth sites are largely hidden in visible light. Thanks to a new generation of infrared and submillimetre space telescopes this veil has been lifted, and a complete picture of starbirth in the Universe is emerging. They reveal an extraordinary diversity of activities in galaxies, and an emerging history of star formation cosmic time, extending back to some of the first stars and seeds of galaxies. This talk will summarise what we have learnt about starbirth on cosmic scales, and highlight the challenges and opportunities which lie ahead.

90% of the atoms are Hydrogen

Can be present as Molecular, H_2, Atomic, H I, or Ionized, H II

Observations of all 3 phases may be required to build a complete picture. The dominant state of regions, and indeed of the whole Universe, has changed over time.

Measurement of the 3 different states of hydrogen sample different physical conditions and use different techniques.

- Molecular hydrogen can be probed at mid/near-IR (vib-ro) or UV (electronic) wavelengths. But its lack of dipole moment gives weak emission and so CO is often used as a proxy.
- Atomic hydrogen is probed using the 21cm line and Lyman absorption lines
- H II is measured via hydrogen recombination lines and free-free emission.

21cm Hyperfine transition in H

- Spin-flip transition in the ground state of Hydrogen. 1420MHz, 21cm
- Very low probability: A ~3 x 10^{-15} sec^{-1}
  Predicted in 1944, first detected in 1951
- But vast clouds of Hydrogen make it easily detectable – a tracer of neutral Hydrogen in our (and other) Galaxy
- Potentially very important for tracing the ionization conditions in the early Universe

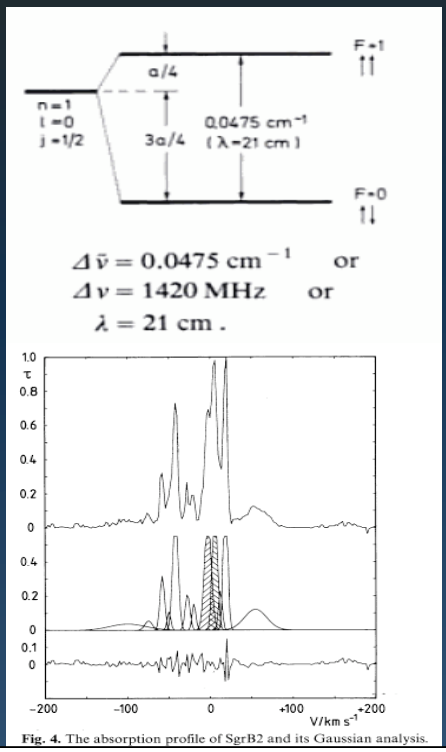

Fig. 4. The absorption profile of SgrB2 and its Gaussian analysis.

The 21cm H line

With A = 2.85 x 10^{-15}, lifetime of the upper state is ~3 10^{14} s or 10 Myr.

The critical density is extremely low n_{crit} ~ 10^{-5}cm^{-3} and so collisional excitation ensures that H is in thermal equilibrium throughout the ISM.

The hyperfine levels have F= 1 and 0, giving statistical weights of 3 and 1 for the upper and lower states respectively.

With ΔE = hν = 1.4x10^{9} h, hν/kT = 0.068/T and so the exponential term is very small everywhere, such that

$$\frac{N_1}{N_0} = \frac{g_1}{g_0} e^{-(\Delta E/kT)} \approx 3 \quad and \quad N_H = N_0 + N_1 \approx 4N_0$$

21cm Emission Brightness

The line emissivity $k_{u,l}$:

$$k_{ul} = \frac{g_u}{g_l} \frac{N_H}{4} A_{ul} h\nu$$

So that in the optically thin case, for the 21cm line the intensity per unit solid angle is

$$I_\nu = \frac{3}{16\pi} A_{ul} h\nu \int N_H dl$$

So we can determine directly the column density of atomic hydrogen along the line of sight by measuring the brightness of the 21cm line (for an isothermal population) integrated over the line profile

Emission and Absorption

It has been used to map out the distribution of atomic hydrogen throughout the galaxy.

Because it has such a small transition probability, the natural width is very small, so velocity structure can be measured in detail

The 21cm line can also appear in absorption against a background source with $T_B > T_S$.

The ISM has cold clouds immersed in a diffuse warmer medium. The cold clumps produce absorption spectra against a warm background.

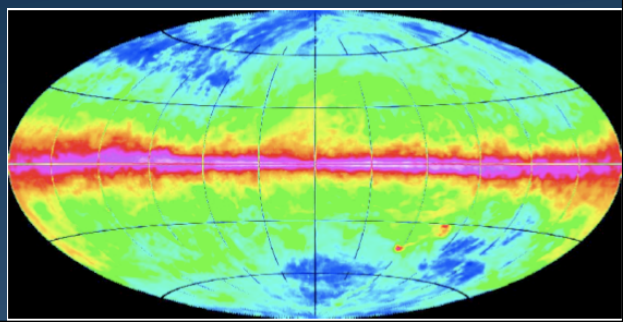

From Dickey et al 2000

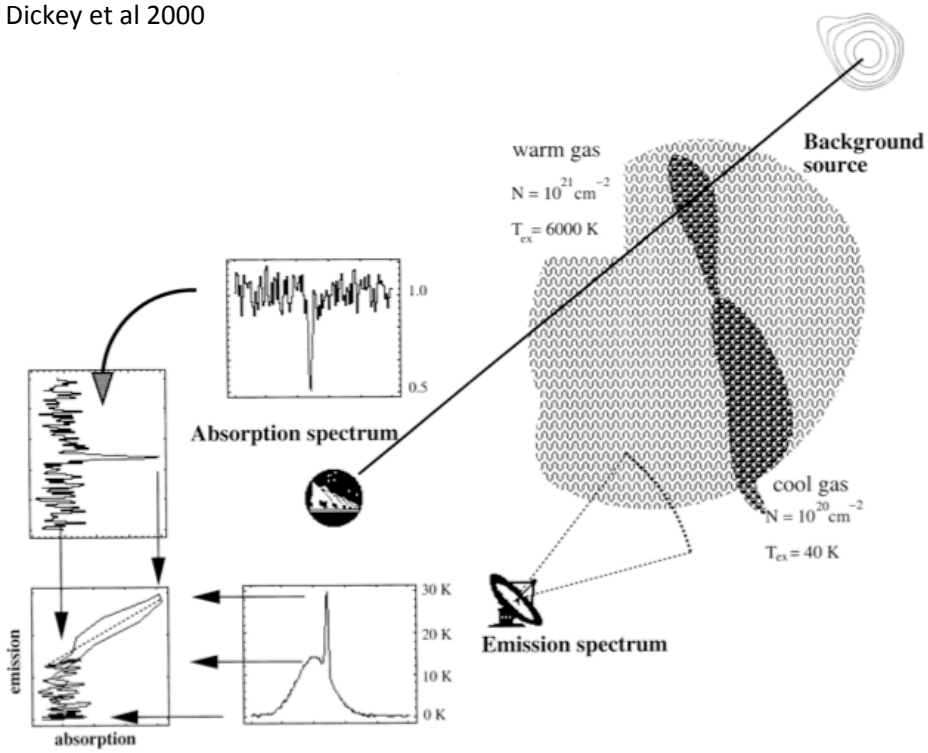

FIG. 15.—Cartoon showing how the emission-absorption diagrams of Fig. 16 are drawn. In this case, the emission spectra are taken with a combination of Parkes and Compact Array telescopes, and there is no offset between the emission and absorption spectra, although the emission spectra correspond to a much larger solid angle than the area of the background source. The "ridgeline" of the feature shown on the graph in the lower left is indicated by the dashed line. This line has slope, m, given by eq. (8) and intercept T_{ew}.

N157b – a supernova remnant in the LMC

Emission (top) and absorption spectra towards N157b in the LMC. Note the weak absorption at V~ 260 and 285 km/s attributed to cool condensations (T~30 K) [from Mebold et al 1997]

The emission spectra widths are generally broader than the absorption spectra, giving a picture of cold clumps within a more diffuse warm medium

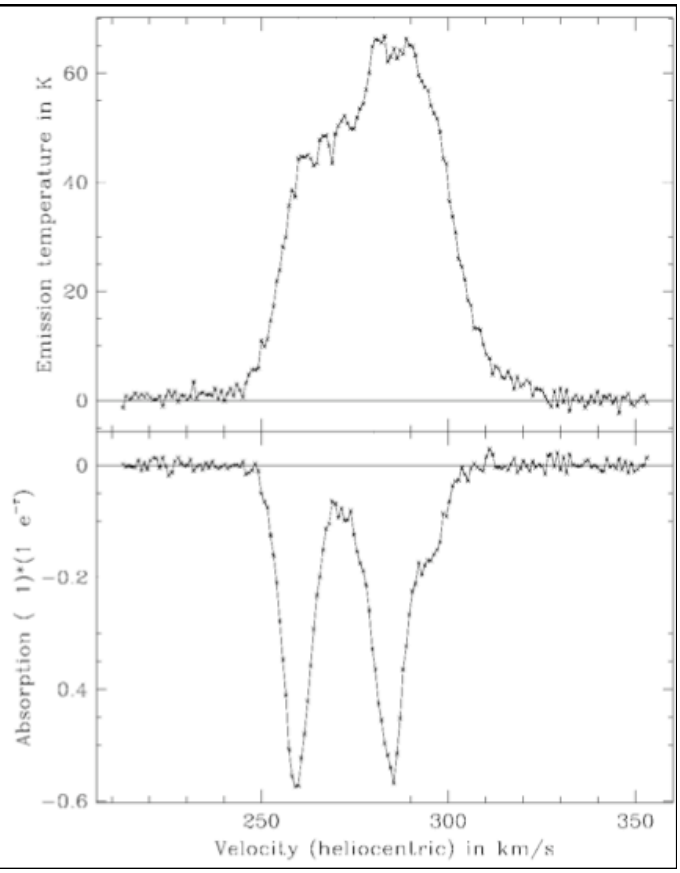

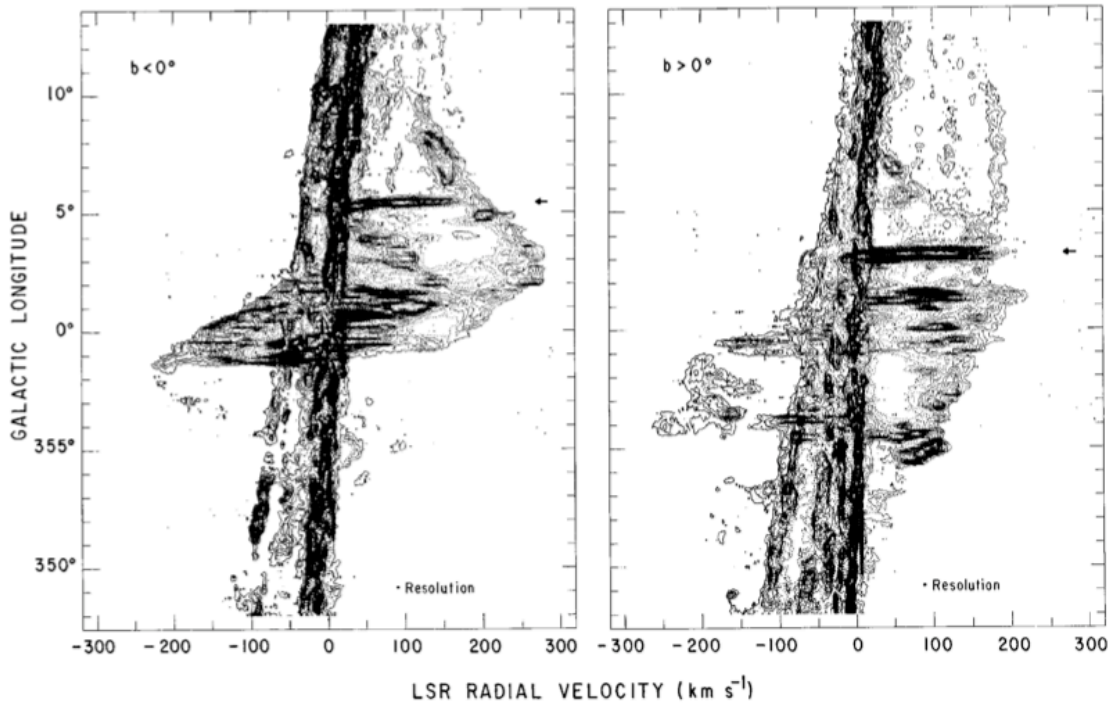

Fig. 5. Two longitude-velocity diagrams integrated below and above the galactic plane. The contour interval is 2 K, with the lowest contour at 2 K. The arrows point to two intense sources with unusually large velocity widths

Galactic Structure

- Long wavelength lines (CO, 21cm, masers) can be measured throughout our Galaxy and used as probes of Galactic structure
- If we start with a simple model of circular orbits, the radial velocities measured can be interpreted as distances.
- The Galactic centre is ~8kpc from the sun, and the sun orbits the Galaxy at 220km/s
- Radial component of velocities are $R_\odot\omega_\odot \sin\gamma$ for the sun and $R_g\omega_g \sin\delta$ for a gas cloud in orbit at radius R
- Giving a differential radial velocity of $(\omega_g - \omega_\odot) R_\odot \sin\gamma$
- The velocity reaches a maximum at the tangent point, and coherent structures can be traced as a position of Galactic latitude and longitude

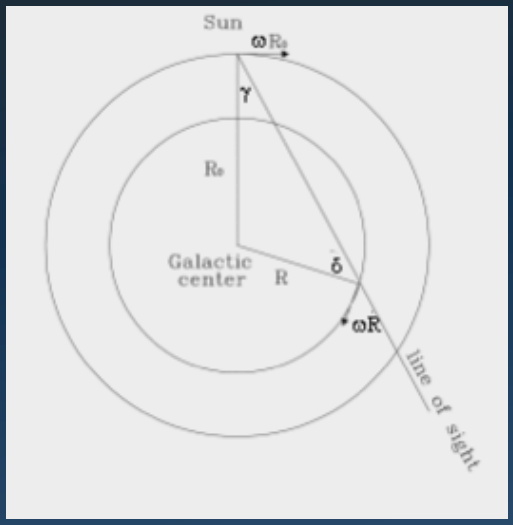

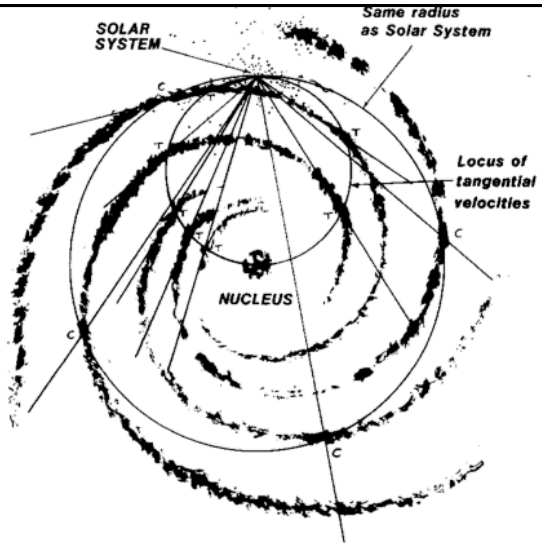

Fig. 1. Plan view of the galactic plane showing tangential points (T) and crossings of the $R/R_0 = 1$ circle (C) derived from CO and H I observations. These points define a geometrical framework for spiral structure. Also sketched on the figure are spiral arms with pitch angle $12° \pm 1°$ derived from the observations. The dots in the vicinity of the solar system show the location of OB associations.

- 21cm and CO maps have delineated major Galactic features – spiral arms, HII regions etc., separating different kinematic structures
- For individual objects there can be ambiguity between near- and far-distances

H_2 : Molecular Hydrogen

H_2 is a symmetric, homonuclear molecule with no dipole moment, so it is a very inefficient radiator, emitting only weak quadrupole transitions, $\Delta J = 2$. Its small moment of inertia means its energy levels are widely-spaced and inefficiently populated at the low temperatures typical of quiescent molecular clouds.

It can be traced using weak pure rotational transitions in the mid-IR, or via ro-vibrational transitions in the near-IR in photo- or shock-excited regions.

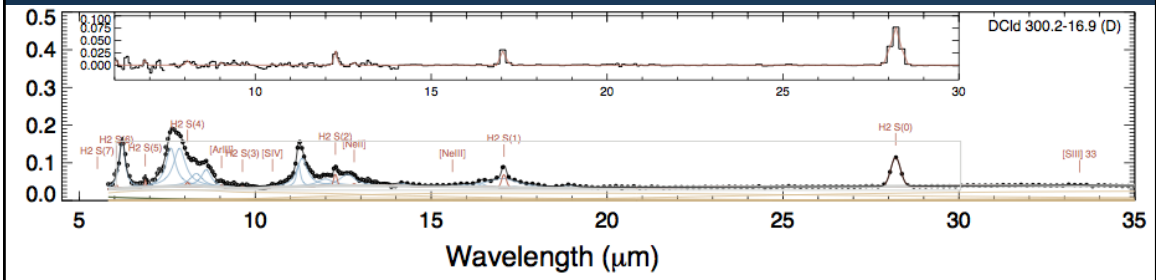

S(0), S(1) and S(2)Pure rotational lines of H2 detected in a translucent cloud by Ingalls et al 2012

Carbon Monoxide : CO

To trace molecular gas in the ISM, observations of CO are usually used as a proxy for H_2. CO is the next most abundant molecule and has bright lines at microwave frequencies.

It can be used to trace cold gas, but relies on a conversion factor from CO to H_2 mass, and has been detected in host galaxies of some of the most distant QSOs

The most common isotopomer $^{12}C^{16}O$ may be very optically thick so rarer isotopes are often used to trace kinematics

Many other molecules can also be used, tracing different environments and different chemistries.

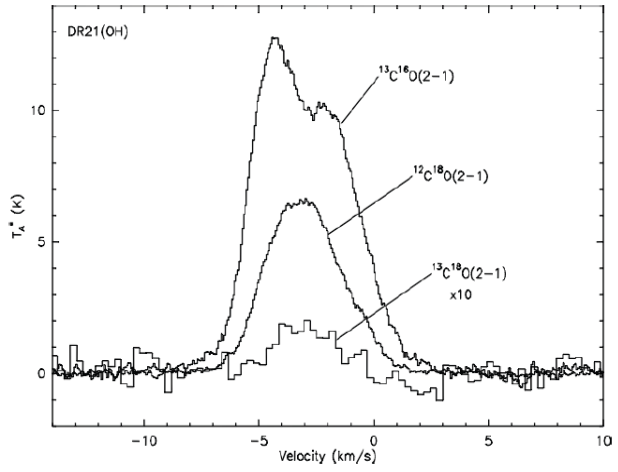

Figure 6-1 - Spectra of the $J = 2 \rightarrow 1$ rotational transition from the $^{13}C^{16}O$, $^{12}C^{18}O$, and $^{13}C^{18}O$ molecular species in the DR21(OH) star-forming region. Note that the $^{13}C^{18}O$ spectrum temperature is multiplied by a factor of ten (adapted from Hezareh et al. 2008, ApJ,

Herschel and ALMA : excitation of CO

Can determine excitation of molecular gas
- photons from HII regions,
- X-rays from AGN,
- Shocks

e.g. the obscured Seyfert galaxy Mkn 231 has strong CO emission beyond J=13, indicating that X-ray excitation is important

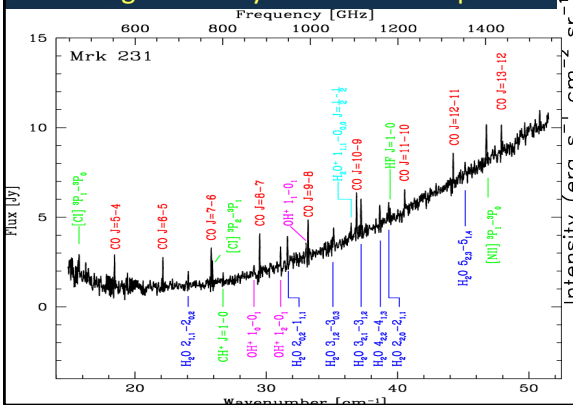

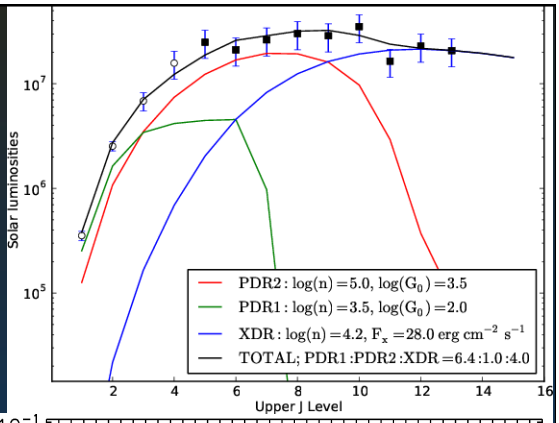

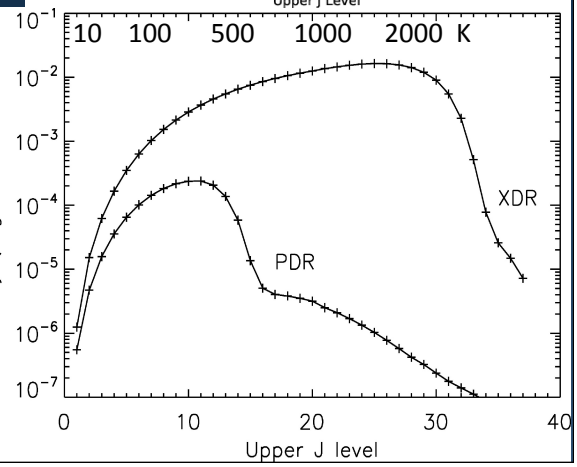

Table 1 Detected interstellar molecules[a,b]

H_2[c,d]	CF^+	SiCN	C_4H^-	CH_3NH_2
AlF	C_3[e,f]	AlNC	HC_2NC	c-C_2H_4O
AlCl	C_2H	SiNC	HCOOH	H_2CCHOH
C_2[d,e]	C_2O	HCP	H_2CNH	CH_2CHCN
CH[e]	C_2S	c-C_3H	H_2C_2O	CH_3C_3N
CH^+[e]	CH_2[d,f]	l-C_3H	H_2NCN	$HC(O)OCH_3$
CN[e]	HCN[f,g]	C_3N	HNC_3	CH_3COOH
CO[c,d,f]	HCO	C_3O	SiH_4	C_7H
CO^+	HCO^+	C_3S	H_2COH^+	H_2C_6
CP	HCS^+	C_2H_2[c]	HC_3N	CH_2OHCHO
SiC	HOC^+	NH_3	C_5H	CH_2CCHCN
HCl[d]	H_2O	HCCN	l-H_2C_4	CH_3C_4H
KCl	H_2S	$HCNH^+$	C_2H_4	CH_3CH_2CN
NH[e]	HNC	HNCO	CH_3CN	$(CH_3)_2O$
NO	HNO	HNCS	CH_3NC	CH_3CH_2OH
NS	MgCN	$HOCO^+$	CH_3OH	HC_7N
NaCl	MgNC	H_2CO	CH_3SH	$CH_3C(O)NH_2$
OH[d,f]	N_2H^+	H_2CN	HC_3NH^+	C_8H
PN	N_2O	H_2CS	HC_2CHO	C_8H^-
SO	NaCN	H_3O^+	NH_2CHO	CH_3C_5N
SO^+	OCS	c-SiC_3	C_5N	$(CH_3)_2CO$
SiN	SO_2	CH_3[c]	l-HC_4N	$(CH_2OH)_2$
SiO	c-SiC_2	C_5	c-H_2C_3O	CH_3CH_2CHO
SiS	CO_2[c]	C_4H	C_6H	HC_9N
CS	NH_2[c]	l-C_3H_2	C_6H^-	CH_3C_6H
HF[c,f]	H_3^+[c]	c-C_3H_2	CH_3C_2H	$HC_{11}N$
SH	H_2D^+	H_2CCN	HC_5N	
O_2[g]	HD_2^+	CH_4	CH_3CHO	

For up to-date lists of detected molecules see:
http://www.ph1.uni-koeln.de/vorhersagen/
http://www.cv.nrao.edu/~awootten/allmols.html

C – detected in the IR
D -detected in the UV
E -detected in the visible
G – detected in the sub-mm

All others found in the radio (from Snow & Bierbaum 2008)

Molecular Transitions

Electronic, vibrational and rotational transitions have large energy differences so that the effects are very largely decoupled (Born-Oppenheimer approximation).
These transitions occur in the UV/optical, near-IR and microwave/radio spectral regions and have their own nomenclature
H_2 has no dipole moment so the vib-rotational transitions are weak, but the electronic transitions can be probed in the UV along sightlines of low extinction.

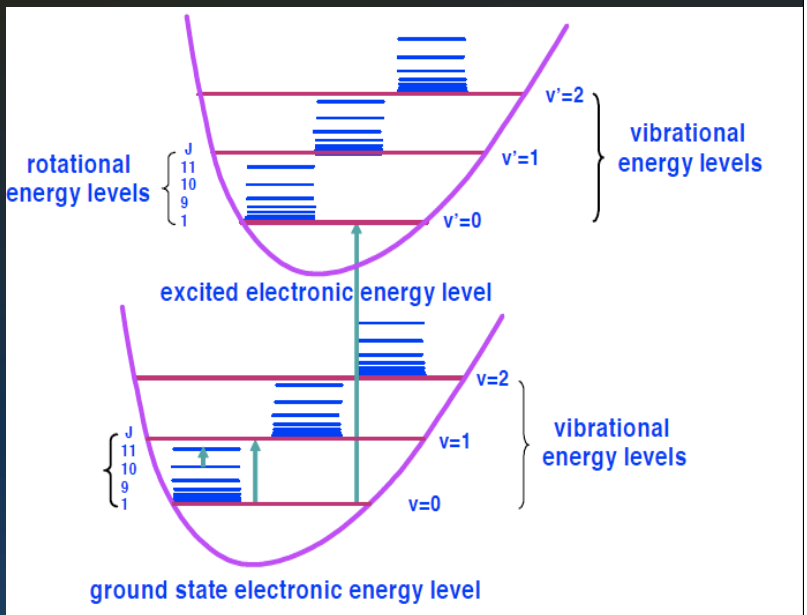

Schematic diagram showing the relative ordering of electronic (purple curves), vibrational (horizontal red lines), and rotational (horizontal blue lines) energy levels. The green arrows show transitions between the various types of energy levels. Quantum numbers associated with the vibrational and rotational energy

H_2 along reddened sight lines (Rachford et al)

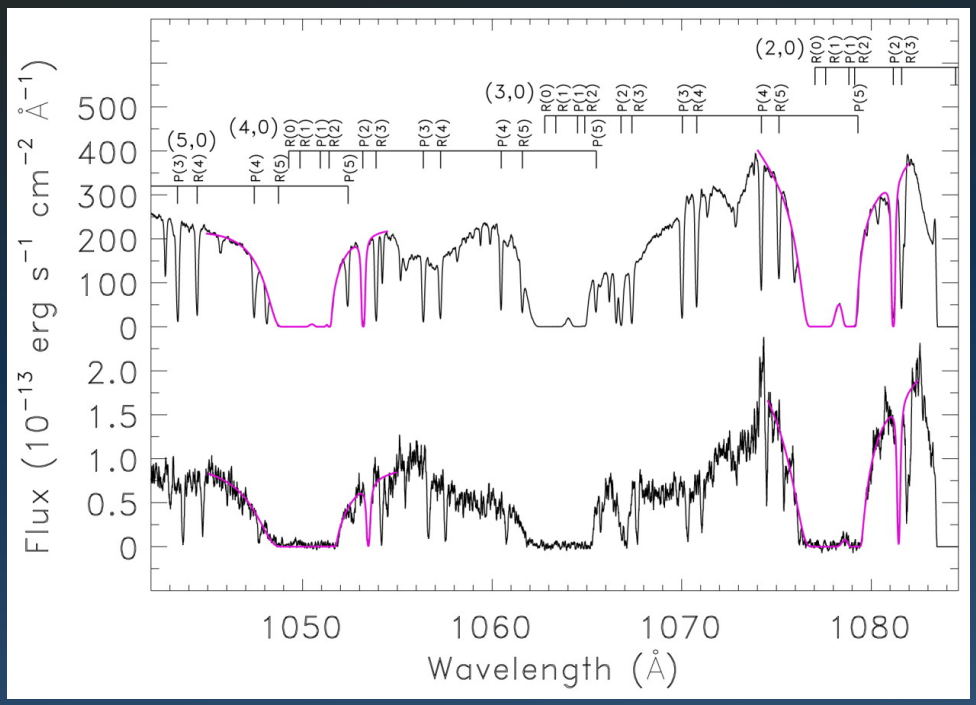

Analysis of H2 line through curve fitting

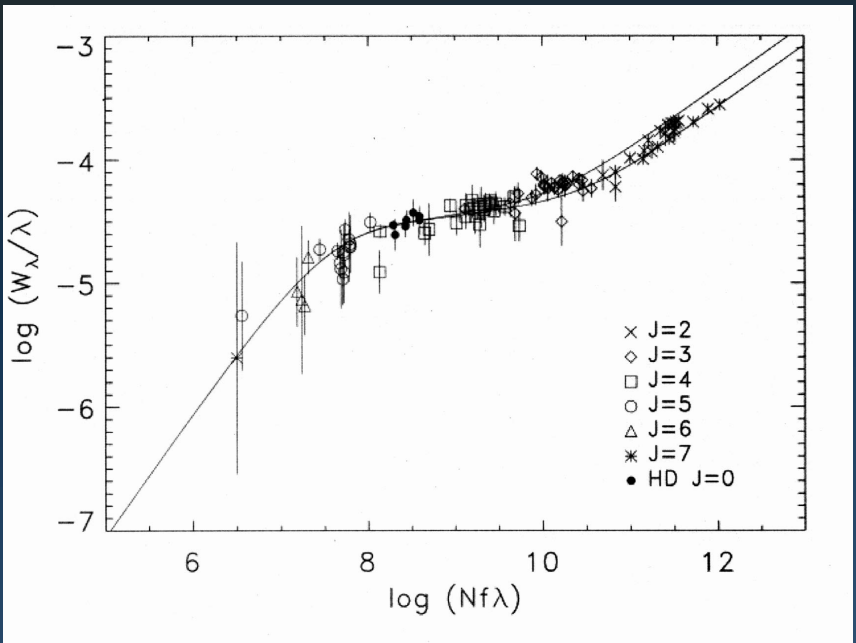

The CO Molecule

The most abundant isotope is ^{12}C + ^{16}O

Rigid rotator harmonic oscillator model:

The molecule rotates about the Centre of Mass at frequency ω

With moment of inertia, $\mathbf{I} = \mu r_0^2$ and r_o is the separation of the nuclei

Rotational Energy = $\mathbf{I}\omega^2/2 = L^2/2\,\mathbf{I}$ which is quantized as:

$$E_{rot} = \frac{J(J+1)\hbar^2}{2I}$$

A transition from rotational level J to J-1 has energy =

$$E_{rot} = \frac{\hbar^2}{2I}(J(J+1) - J(J-1)) = \frac{\hbar^2 J}{I}$$

The minimum excitation temperature is $\sim E_{rot}/k \sim 15K$ for J=2

Characteristic diatomic molecular emission

The rotational transitions associated with each vibrational transition produce a characteristic P and R branch appearance given by ΔJ=-1 and ΔJ=+1

And hence

$\nu = \nu_0 + 2(J+1)B$ for the R branch with J= 0, 1, 2 , 3…. and

$\nu = \nu_0 - 2(J)B$ for the P branch with J= 1, 2, 3…..

where the rotational constant $B = h/8\pi^2 I$

With increasing temperatures, higher rotational and vibrational levels are populated, giving additional lines at higher frequencies.

Different isotopes may be well separated and easily measurable in cold regions where linewidths are small. Transition frequency $\alpha\ \mu^{-1}$ and so the ^{13}CO isotope has frequencies 5% lower than ^{12}CO. Massive, large molecules emit at lower frequencies than compact, light species.

Vibration-Rotation Transitions

Low frequency transitions from cold gas.

For CO, the main tracer of molecular gas, the ground state rotational transition J=1-0 is at 2.6mm, whilst the 1-0 vibrational transition is at 4.7μm.

The low-lying lines can be very optically thick, and so the isotopes ^{13}CO or $C^{18}O$ often provide better estimates of column density, though subject to assumptions on isotopic ratios.

Different molecules preferentially probe different physical and chemical conditions.

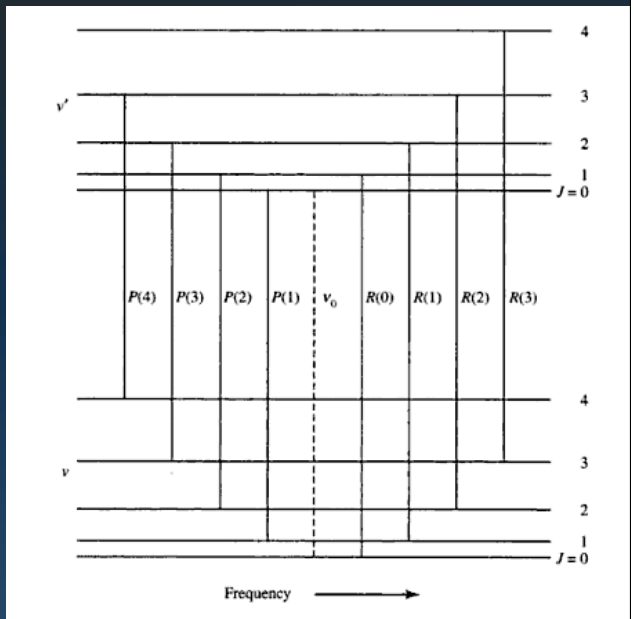

Figure 7.5
A schematic diagram illustrating the *P* and *R* branches of the vibrational–rotational transitions of a diatomic molecule.

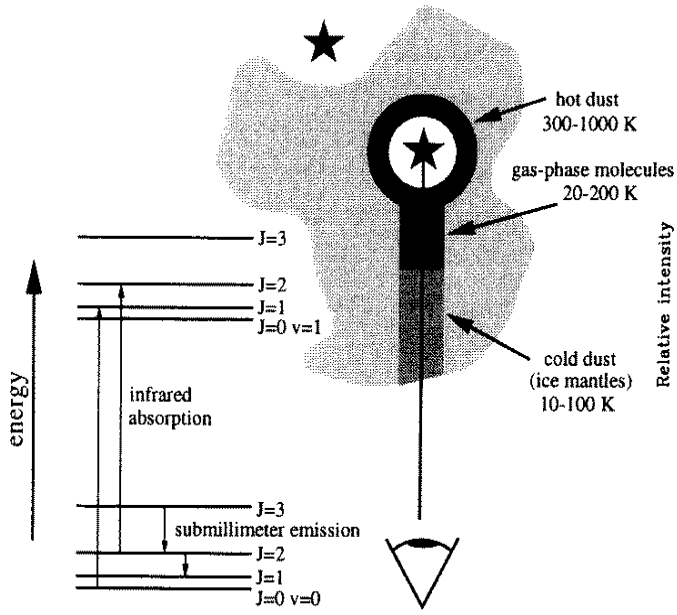

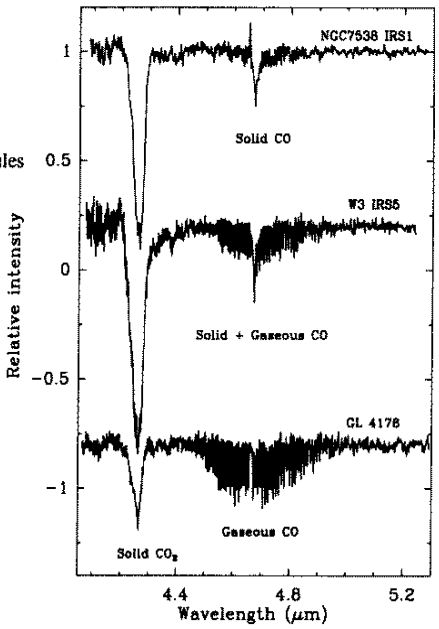

Carbon Monoxide probed through microwave rotational transitions or vib-rotational near-IR transitions. In the cores of dense cold clouds, CO condenses as ice.

Silicon Monoxide Δv=1 Fundamental Band

The Δv=1 fundamental ro-vibrational band of SiO is at 8.1μm

Each vibrational level has rotational structure, leading to the P- and R-branches typical of a vib-rot band.

With a model anharmonic oscillator the emission from each rotational level, J, is given by

$$I = C(J' + J'' + 1)\, e^{-B'J'(J'+1)\,hc/kT}.$$

where B and C are molecular constants and J', J" are the lower and upper levels

The rotational and vibrational level populations depend on the temperature and are reflected in the profile of the band

In SN 1987A, the band profile indicates T~1500K for a thermal population

and with $$I_\nu = \frac{1}{4\pi d^2} \int h\nu A_{ij} N_i dV$$ the mass of SiO ~ 4 x10^{-6} M_o on day 500

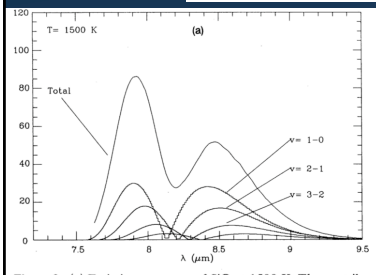

Figure 2. (a) Emission spectrum of SiO at 1500 K. The contributions from the $v = 1, 2, 3$ and 4 levels for $\Delta v = 1$ are shown together with the total band emission.

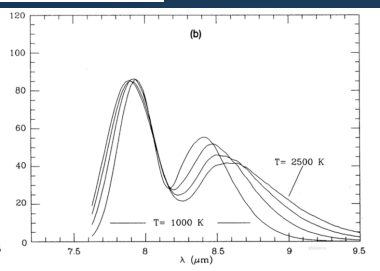

Figure 2. (b) A comparison of the normalized SiO emission profiles for excitation temperatures of 1000, 1500, 2000 and 2500 K, degraded to the instrumental resolution of the UCL spectrometer.

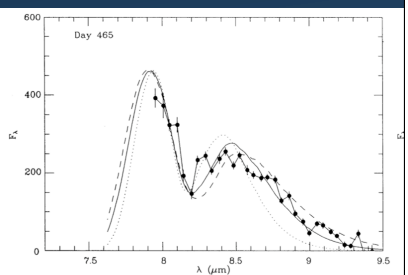

Figure 3. Observed SiO emission bands from SN 1987A on day 465 and resent the model SiO emission at $T = 2000$, 1500 and 1000 K respectivel

Silicon Monoxide Masers

Maser emission can occur when the population in an excited state is higher than in the lower state, and stimulated emission leads to amplification

Silicon Monoxide shows bright maser emission in the V=1, J=1-0 and V=1, J=2-1 transitions.

The population inversion can be caused by pumping by infrared photons into higher excited levels and/or collisional excitation. Locket & Elitzur (1992 ApJ 399, 704) argue that collisions with H_2 in dense (N~ 10^9 cm^{-3}) clumps are the dominant SiO maser pump mechanism

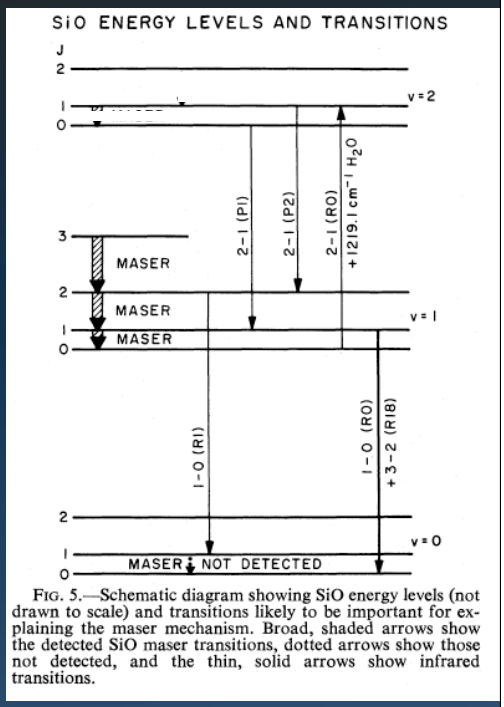

FIG. 5.—Schematic diagram showing SiO energy levels (not drawn to scale) and transitions likely to be important for explaining the maser mechanism. Broad, shaded arrows show the detected SiO maser transitions, dotted arrows show those not detected, and the thin, solid arrows show infrared transitions.

Stimulated Emission

In the inverted population, one of the electrons randomly jumps to the lower energy level. It emits a photon which passes another atom stimulating the release of another photon. Because their release was stimulated, the group of photons has unique properties and leads to very high gain.

To achieve this needs a dense medium with a large population of SiO molecules in excited states, and small velocity dispersions.

This can be found in the hot inner regions of circumstellar dust shells

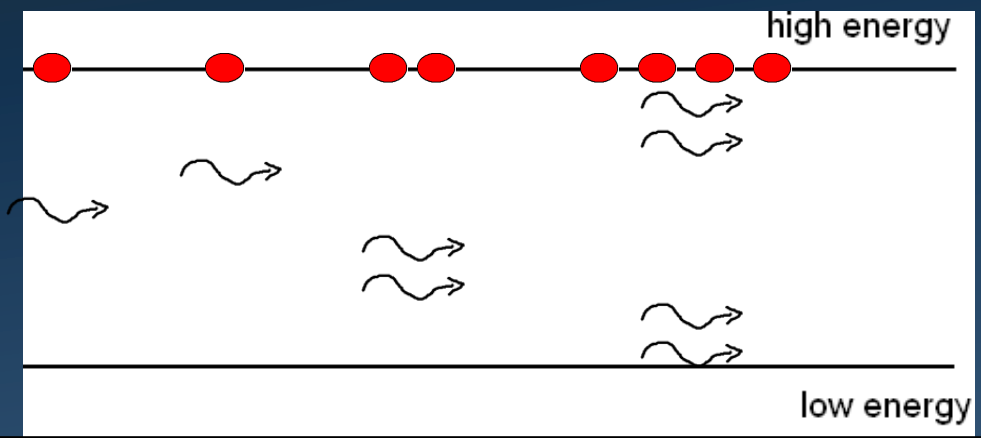

SiO Maser emission in TX Cam

A Mira variable star with a dense extended dust shell.

The maser emission arises predominantly in the inner regions of the stellar shell where T~1500K and varies as the star pulsates.

Movie from VLBA observations over several months

Masers occur in regions of high density, but below n(crit) so that collisional de-excitation of the excited level is not dominant.

(Diamond & Kemball 2002 ApJ 599, 1372)

CO at high redshift in SDSSJ12143912.04+111740.5 (Srianand et al 2008)

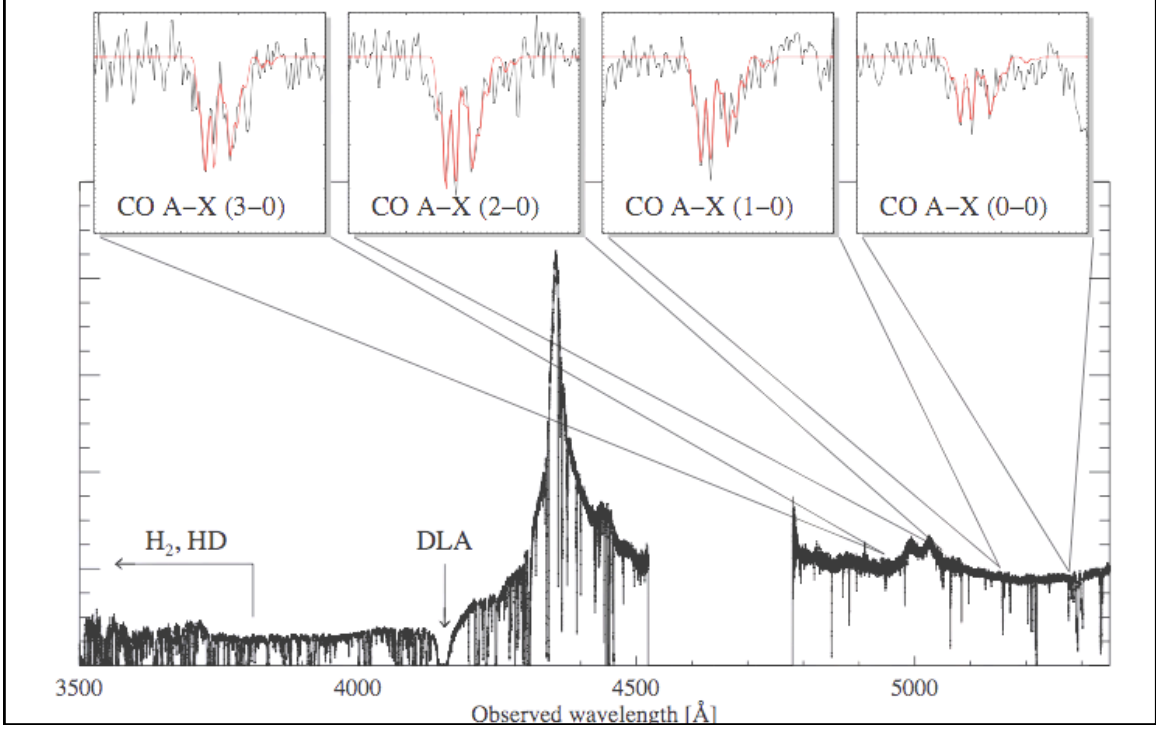

Excitation temperature at z= 2.42

The UV electronic transitions can be used to estimate the temperature of CO molecules

The CO excitation diagram for ***SDSS J143912.04+111740.5***

A straight line with slope $1/(T_{ex}\ ln\ 10)$ *indicates thermalization of the levels. The diagram is given for the main CO component at zabs = 2.41837. The three lines give the mean and 1σ range obtained from T01 , T02 , and T12 . The diagram is compatible with thermalization by a black-body radiation of temperature 9.15 ± 0.72 K when TCMBR = 9.315 ± 0.007 K (long dashed line) is expected at zabs = 2.4185 from a hot big-bang.*

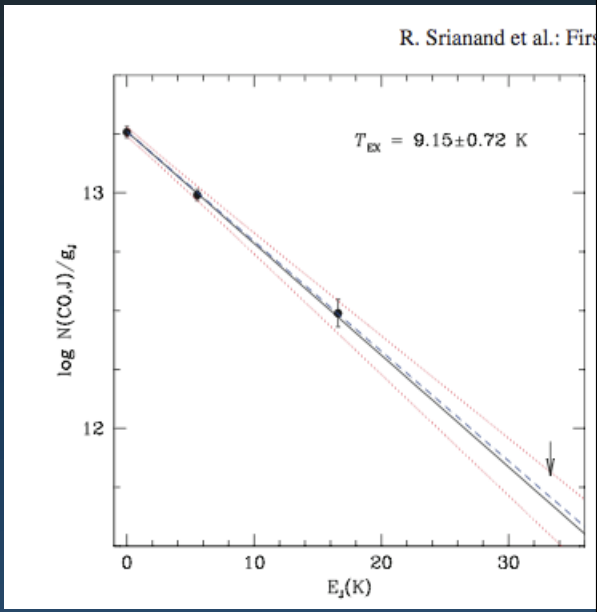

The Gaseous ISM

Is a dynamic environment with different constituents, with complex chemical and photo-processing.

Using the techniques described, we can analyse spectral observations to estimate the dynamics, excitation, temperature, density, abundances of the atomic, molecular and ionic gas to examine the chemical processes and enrichment of the ISM. We can do this as functions of position and time within our own and other galaxies and the interstellar and intergalactic medium.

New facilities are opening up the molecular Universe to study and undoubtedly many new discoveries await.

Measurements of gas phase abundances are used to infer depletions of refractory elements, which impose severe constraints on the composition of dust particles.

The ALMA Observatory, located at 5000m in the Chilean Altiplano, explores the molecular content of the universe in unprecedented detail. Construction of the array was completed in 2014.
Astrochemistry is a complex and rapidly-growing discipline seeking to understand the composition and processes that lead to the rich molecular spectra being detected.
Many lines remain unidentified at the moment.

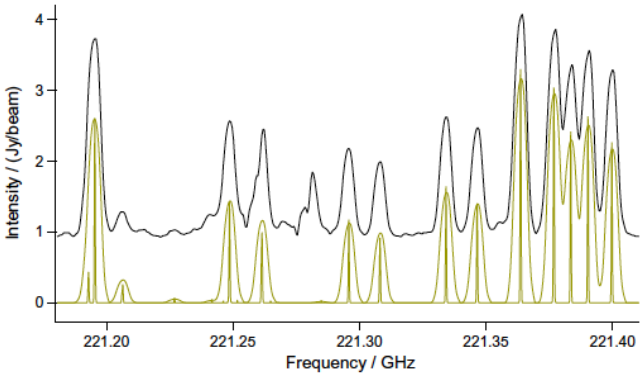

ALMA Spectrum of Orion KL, the current star-forming region NW of the Trapezium stars in the Orion nebula

Fig. 5. Spectral comparison in the region of a methyl cyanide $\nu_8 = 1$ bandhead. The upper black trace is ALMA and the lower gold trace a CES LTE simulation at 190 K, including effects of optical thickness. Also in gold is a stick spectrum that shows methyl cyanide at laboratory resolution.

Initial ALMA results on SN1987A

25 years post explosion,
CO Mass >0.01M(sun) at T~ 14K – implies CO has continued to form along with other molecules, e.g. SiO and increased dust condensation
Further measurements can yield isotopic ratios which may constrain supernova explosion models.

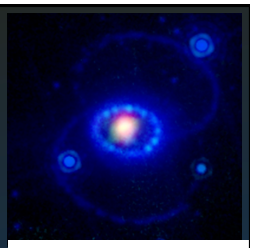

HST (blue) and ALMA CO (red) image of SN1987A

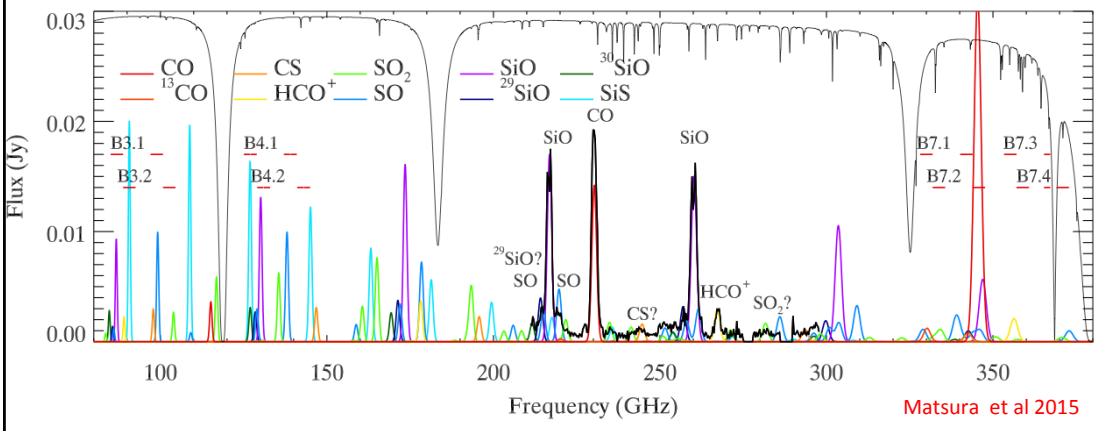

Matsura et al 2015

Figure 1: *Observed ALMA SN 1987A spectrum (thick black line) with molecular spectra model*